AB INITIO CALCULATIONS OF RELATIVE STABILITIES OF DIFFERENT STRUCTURAL ARRANGEMENTS IN DIOCTAHEDRAL PHYLLOSILICATES

DANIEL TUNEGA[1,2], BERNARD A. GOODMAN[2,3,*], GEORG HABERHAUER[2], THOMAS G. REICHENAUER[2], MARTIN H. GERZABEK[4] AND HANS LISCHKA[1]

[1] Institute for Theoretical Chemistry, University of Vienna, Währingerstrasse 17, A-1090 Vienna, Austria
[2] Department of Environmental Research, Austrian Research Centers GmbH − ARC, A-2444 Seibersdorf, Austria
[3] Department of Natural Resources and Environmental Sciences, University of Illinois at Urbana-Champaign, Urbana, IL 61801, USA
[4] Institute of Soil Research, University of Natural Resources and Applied Life Sciences, Peter-Jordan-Strasse 82b, A-1190 Vienna, Austria

Abstract—An *ab initio* theoretical approach has been used to calculate optimized geometries and the relative energies of various compositional arrangements in structures of dioctahedral smectites based on models consisting of two unit-cells. These calculations indicate that the energy differences between structures having vacancies in sites with *cis*- or *trans*-OH coordination are small and that their relative energies vary with the chemical nature of the substitutions. For example, a *cis*-OH coordination for the vacancy was the most stable when the interlayer charge originated from substitution of Al for Si in the tetrahedral sheet, whereas the *trans*-coordination was the more stable for most cases of substitution in the octahedral sheet, an exception being Fe(II) for Al where the *cis*-OH coordination was favored. It seems likely, therefore, that long-range structural disorder will be a common phenomenon in natural phyllosilicate specimens.

Key Words—*Ab Initio*, Dioctahedral, Phyllosilicates, Smectite, *Cis*- and *Trans*-coordination.

INTRODUCTION

The phyllosilicates are a class of minerals with both industrial and environmental significance. They are often of small particle size (*i.e.* clay minerals) and have important catalytic properties as well as making major contributions to the physical and chemical properties of soils. Phyllosilicate minerals of the 2:1 type are layer structures in which planes of cations coordinated octahedrally to oxygen atoms are sandwiched between two sheets in which the cations have tetrahedral coordination (Bailey, 1980). In the octahedral sheet, 1/3 of the oxygen atoms are in the form of hydroxyl groups, which form coordination bridges to neighboring octahedral cations, whilst the remainder of the oxygen atoms form links between the octahedral and tetrahedral sheets. Structures in which all of the octahedral sites are occupied are referred to as trioctahedral, whereas dioctahedral structures have 1/3 of these sites vacant.

A characteristic of phyllosilicate minerals is their ability to accommodate a wide range of isomorphous substitutions in both the octahedral and tetrahedral sheets. Typical substitutions are Al or Fe(III) for Si in tetrahedral sheets, or various di- and trivalent ions, including Fe(II) and Fe(III), in the octahedral sites. These substitutions often result in an imbalance between the anionic and cationic charges in the structures with the production of an excess negative layer charge on the aluminosilicate layer. This charge is compensated by the incorporation of cations between layers. The component layers in the structures are, therefore, mainly held together by attractive Coulombic forces between negatively charged layers and interlayer cations. Thus the smaller the layer charge, the easier it is to separate layers. As a consequence, structures with small interlayer charge can exchange interlayer cations (usually in hydrated form) or can intercalate organic molecules. These minerals also have a tendency to swell by the incorporation of large amounts of water molecules. The physical properties of this family of minerals are thus closely related to details of their composition, oxidation states, and arrangements of ions (especially Fe) within the structures (*e.g.* Stucki, 1988).

Because of the combination of compositional disorder and the existence of different arrangements by which layers can stack on top of one another, complete information on the structural and compositional details of individual minerals cannot usually be obtained with diffraction methods, although a few well-defined specimens have been characterized (*e.g.* Drits 2003; Manceau *et al.*, 2000). Also, although a considerable amount of knowledge has been generated by various spectroscopic methods, these results usually require a degree of interpretation and conclusions are seldom completely unambiguous. An example is the extensive debate spanning more than three decades concerning the interpretation of clay mineral Mössbauer spectra.

220

The recent rapid progress in computer technology and advances in bonding theory now allow the inclusion of computer simulation methods as a tool for solving some of the questions on the structural and compositional details of phyllosilicate minerals. A good example of the combined use of theoretical and spectroscopic methods is found in the works of Sainz-Diaz *et al.* (2001a) and Cuadros *et al.* (1999). These authors used an inverse Monte Carlo method to determine the distribution of Al^{3+}, Fe^{3+} and Mg^{2+} in the octahedral sheet of dioctahedral 2:1 phyllosilicates by combining the chemical analytical data with spectroscopic results obtained from Fourier transform infrared (FTIR) and ^{27}Al magic angle spinning nuclear magnetic resonance (MAS NMR) spectroscopies. The intensities of the OH-bending modes in the IR spectra allow the nature and proportion of the different cation pairs bound to the OH groups to be determined. These data indicated Fe segregation by short-range ordering, and this increased with the proportion of illite within illite-smectite phases. The intensity of the ^{27}Al MAS NMR peak is dependent on the Fe distribution and when this information was included in the Monte Carlo calculations, they failed to produce appropriate cation distributions for samples with greater numbers of illite layers and appreciable Fe content. It was concluded that there was long-range Fe ordering that could not be detected by the spectroscopic techniques. However, the NMR intensities are affected by the overall paramagnetic ion content, and the local environments of individual paramagnetic ions. Aluminum atoms close to Fe^{3+} ions in the structure may not be visible because of the large dipolar interaction between the ^{27}Al nucleus and the magnetic moments of the unpaired electrons on the Fe. For example, Morris *et al.* (1990) reported that an Fe centre in an aluminosilicate mineral can completely wipe out the Al signal in ^{27}Al MAS NMR when their separations are <~6 Å. Furthermore, any small errors in the chemical analytical data could have serious implications for the validity of such analyses, as could the presence of traces of Fe oxide minerals (which are commonly associated with phyllosilicate specimens).

Theoretical methods based on empirical interatomic potentials have also been used in structural studies of phyllosilicates with various types of substitutions (Skipper *et al.*, 1995; Bosenick *et al.*, 2001; Teppen *et al.*, 1997; Sainz Diaz *et al.*, 2001a, 2001b, 2001c, 2003a, 2003b, 2004; Palin *et al.*, 2004). Features such as interlayer spacing, hydrogen bonding, and weak van der Waals interactions are very sensitive to the empirical potentials used, and the calculated results are often of a poor quality. Thus, reproduction of these sensitive features needs methods based on quantum-mechanical theory. Nevertheless, Sainz-Diaz *et al.* (2001b) successfully modeled the crystal structures of pyrophyllite, muscovite, margarite, beidellite, montmorillonite and various smectites and illites. In smectite-illite samples,

the effects of cation substitutions in both octahedral and tetrahedral sites were investigated and were found to be consistent with experimental data where these were available. Sainz-Diaz *et al.* (2001c) also used a similar approach to model the distribution of the vacancies in the octahedral sheet of illites and smectites. A wide range of compositions was studied with various octahedral, tetrahedral and interlayer charges being generated through the cation substitutions (Mg^{2+}, Fe^{3+} for Al^{3+} and Al^{3+} for Si^{4+}). Unit-cell parameters were calculated for structures in which the vacancy had *cis*- or *trans*-OH coordination (Sainz-Diaz *et al.*, 2001b, 2001c). In most cases the energy difference between these states was small, and the authors concluded that natural samples would often consist of a mixture of these phases. They found that the configuration in which the vacancy had *cis*-OH was most stable at the smectite end of the illite-smectite series, as observed experimentally (Drits *et al.*, 1998; Drits, 2003), whereas the configuration with a *trans*-OH vacancy was most stable in structures with high Mg^{2+} or Fe^{3+} content, as reported experimentally for illite-smectite (McCarty and Reynolds, 1995) and nontronite (Manceau *et al.*, 2000). Sainz-Diaz and coworkers continued their studies of octahedral cation distributions in smectites and illites also by means of *ab initio* methods (Sainz-Diaz *et al.*, 2002; Timon *et al.*, 2003; Botella *et al.*, 2004).

All above-mentioned studies were based on bulk models, and in cases where empirical potentials were applied, the quality of the potential parameters was controlled by structural parameters, which were related to available experimental data. These papers have not only added greatly to our understanding of the locations of cations and vacancies in the structures of various aluminosilicate minerals, but also to the stacking of layers in the various sheet silicate minerals. The approach in most of these publications has made use of experimental data from both analytical and physical techniques and these have 'guided' the selection of the empirical parameters. The main strength of this approach is that the computations are sufficiently simple to allow extended structures to be studied, but potential problems arise if there are errors in any of the experimental data, or if the various measurements are made with non-identical samples.

Although, as discussed above, well-fitted empirical parameters can give a good agreement between model structural and experimental data, investigations of ordering of cation substitutions within layers, especially in the short range, needs *ab initio* electronic calculations. This is because changes in the electron structure around the central cations have the dominant effect on the stability of the layers, a process which is even more important in the case of open shell cations, such as Fe^{2+} or Fe^{3+}, than with closed shell cations, such as Al^{3+} or Mg^{2+}. The electronic structure of these open-shell cations cannot be gained from calculations with any

type of empirical interatomic potentials. Thus full electronic calculation is unavoidable in studies of Fe^{II}/Fe^{III} redox process in Fe-rich phyllosilicates. The computational requirements of *ab initio* methods are much greater than those using empirical parameters, making it very difficult to investigate long-range phenomena, but they are not subject to problems of possible inaccuracies in experimental data.

Ab initio methods based on density functional theory (DFT) with incorporated periodic boundary conditions have previously been applied to studies of structures and properties of various phyllosilicates (Smrčok and Benco, 1996; Bridgeman *et al.*, 1996; Hobbs *et al.*, 1997; Benco *et al.*, 2001; Stixrude and Peacor, 2002; Tunega and Lischka, 2003). The strength of *ab initio* calculations was demonstrated by McConnell *et al.* (1997), who showed that empirical potentials lead to an overestimation of the Coulombic energy term (by ~30%) compared to the *ab initio* model in determinations of the enthalpy of disorder for exchange between tetrahedral Al and Si in simple aluminosilicate structures. Density functional theory was also used by Tunega and Lischka (2003) to investigate the Si/Al distribution in the tetrahedral sheets of vermiculite.

In the present work we investigate a dependence of energetic stabilities of isolated smectite-like layers on different cation distributions. Calculations have been made of the relative energies of structures in which the vacancy is located in sites with *cis*- or *trans*-OH coordination. Consideration is also given to structures in which the layer charge originates from isomorphous substitutions in cationic sites with either octahedral or tetrahedral coordination. In addition, in the structure with the vacancy having *cis*-OH coordination and the layer charge originating from substitution of Al in an octahedral site by a divalent ion (Mg^{2+} or Fe^{2+}), the relative energies are calculated for this ion being located in sites with *cis*-OH *vs. trans*-OH arrangements. The changes in the electronic structure of layers are shown on calculated Mulliken atomic charges.

METHODOLOGY

Phyllosilicate models

There are no accurate experimental atomic positions for smectite minerals. The starting geometries for our models were derived from the structural models for the 2:1 dioctahedral illites-smectites assuming a general formula $(Al,M)_4(Si,T)_8O_{20}(OH)_4$ proposed by Tsipursky and Drits (1984). The initial computational cell dimensions were: $a = 5.162$ Å, $b = 8.980$ Å and $c = 25.0$ Å. The size of the c parameter produces a ~18 Å vacuum between adjacent layers. It means that mutual interactions between layers are negligible and it is justifiable to investigate isolated layers. In the 2:1 dioctahedral phyllosilicates there are two basic arrangements of cations within the octahedral sheets. In one case the

octahedral vacancy is located in sites with *trans*-OH coordination, while in the other it has *cis*-OH coordination (see structural models in Figure 1). Substitutions considered in the octahedral sheet are Al^{3+} by Mg^{2+}, Fe^{2+} or Fe^{3+}, and Si^{4+} by Al^{3+} in the tetrahedral sheet. Both types of layer presented in Figure 1 have four possible positions for the substitution in either the octahedral or tetrahedral sheets (in our simulations we do not consider any symmetrical restrictions so all sites are treated as independent). All sites were mapped with all the cations considered. All calculated structures had only one isomorphous substitution per unit-cell; higher levels of substitution have not been considered in this paper. With one substitution, an excess layer charge of $-1\ |e|$ per unit-cell is produced. In one set of models this charge is not compensated, while in another two sets it is compensated by a Na^+ cation. Details on Na^+ positions in the interlayer space are given later. In addition, a pyrophyllite-like structure (*i.e.* no substitution) was also considered.

Ab initio simulations

The calculations were performed using the Vienna *Ab initio* Simulation Package (VASP) (Kresse and Hafner, 1993; Kresse and Furthmüller, 1996), which is based on density functional theory (DFT). We used parameterization of the local exchange-correlation function according to Perdew and Zunger (1981), and used the generalized gradient approximation (GGA) of Perdew and Wang (1992) to make non-local corrections. A plane-wave basis set using the projector-augmented wave (PAW) method (Blöchl, 1994; Kresse and Joubert, 1999) was used in the calculations. The PAW method combines the advantage of the plane-wave basis set with the accuracy of the all-electron schemes. A cutoff of 400 eV for the basis set was applied in each calculation. The Monkhorst-Pack (1976) scheme was used for the automatic generation of a **k**-point grid. The appropriate number of **k**-points used in subsequent simulations was determined on the basis of calculations performed with the pyrophyllite structure. In the pyrophyllite test calculations, the full optimization (atomic positions plus unit-cell parameters and a cell volume) was performed. The results of these test calculations are documented in Table 1 and are discussed in the following section. Frequencies presented in Table 1 were calculated numerically using a finite-difference technique. Because of the large number of calculations required to cover the various substitutions, we decided to use a $2 \times 2 \times 1$ **k**-point sampling scheme for all other calculations. Two types of structural relaxation were performed. In the first case, full atomic relaxation was allowed within fixed unit-cell dimensions. The unit-cell volume relaxation has no meaning for these calculations as we used the models of isolated layers with the c cell parameter much bigger than the other two. In these cases, relaxation of unit-cell parameters at a constant cell volume was permitted. In all structural relaxation
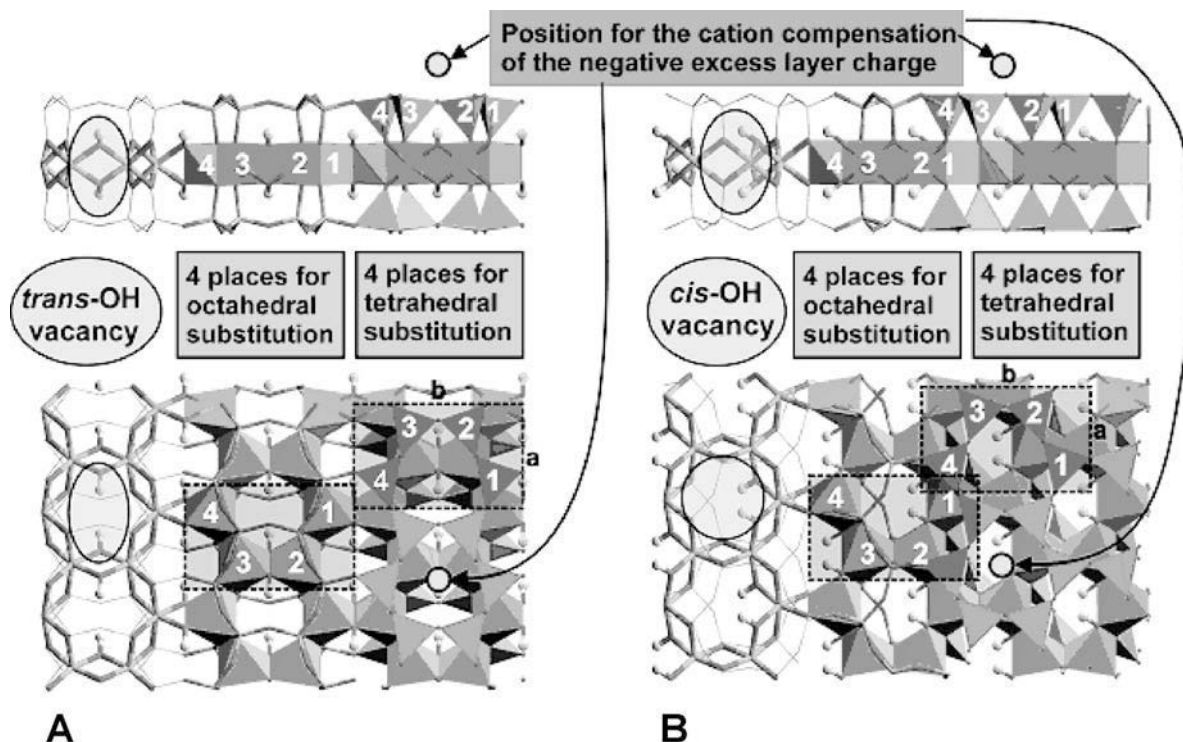
Figure 1. Structures of dioctahedral phyllosilicate minerals with vacancy in sites with (A) *cis*-, and (B) *trans*-OH coordination.

calculations, optimization of atomic positions was performed using a conjugate-gradient algorithm with a stopping criterion of 10^{-4} eV for the total energy and 0.01 eV/Å for the rms residual force. No symmetry restrictions were applied during any relaxation procedure.

As it is not an option to calculate Mulliken atomic charges in the current implementation of the VASP program, we used the SIESTA program (Soler *et al.*,

2002) from the Fundación General de la Universidad Autónoma de Madrid (FGUAM) for this purpose. This quantum-chemical program uses localized Gaussian atomic basis sets and atomic pseudopotentials. The DFT calculations were performed on the optimized structures obtained from the VASP calculations and the localized atomic basis set of double-zeta (DZ) quality was used in these calculations.

Table 1. Variation of structural parameters and O−H stretching frequency with the number of **k**-points used for calculations with pyrophyllite.

No. of **k**-points	1	2	4	8	32	32[a]	Exp.[b]
Total energy (eV)	−296.9973	−297.0534	−297.0772	−297.0504	−297.0532	−297.1043	−
a (Å)	5.129	5.132	5.130	5.131	5.131	5.229	5.160(2)
b (Å)	8.930	8.909	8.910	8.908	8.908	9.083	8.966(3)
c (Å)	9.137	9.153	9.146	9.151	9.152	9.657	9.347(6)
α (º)	90.89	90.93	90.91	90.91	90.91	91.09	91.18(4)
β (º)	100.60	100.61	100.62	100.59	100.56	100.29	100.46(4)
γ (º)	89.87	89.84	89.84	89.85	89.84	89.72	89.64(3)
V (Å^3)	411.332	411.328	410.849	411.099	411.144	451.232	425.16
d(Si−O)[c]	1.630	1.629	1.628	1.628	1.628	1.633	1.617(11)
d(Al−O)[c]	1.904	1.908	1.907	1.908	1.908	1.928	1.912(17)
d(O−H)[c]	0.970	0.970	0.970	0.970	0.970	0.970	0.971
ν(OH) (cm^{-1})	3743.1	3740.8	3737.2	3739.3	3739.9	3744.1	3675

[a] Cell-volume scaling; relaxation of atomic positions and cell parameters; minimum found at the scaling factor 1.02
[b] Structural data from Lee and Guggenheim (1981), OH frequency from Wang *et al.* (2002)
[c] Mean values of the bond lengths

RESULTS

k-*point sampling*

Optimized structural parameters and stretching vibrations for the inner OH group of pyrophyllite are reported in Table 1 with respect to the number of irreducible **k**-points, and the results are also compared with experimental data. One can see that there are only very small differences between results obtained with 2 **k**-points and 32 **k**-points. On the basis of this comparison, we decided to use $2 \times 2 \times 1$ **k**-point sampling (2 irreducible **k**-points) in all further calculations. The calculated lattice parameters, obtained with full relaxation of atomic positions, and the cell parameters are only slightly smaller than the experimental ones (Table 1). The calculated cell volume is ~3% less than the experimental value. Usually, as was found in other calculations on the pyrophyllite structure (Sainz-Diaz *et al.*, 2002; Refson *et al.*, 2003; Teppen *et al.*, 2002), DFT methods give slightly expanded cells with the largest deviation from experiment being for the *c* lattice parameter. This is explained by the fact that weak dispersion interactions (such as between the pyrophyllite layers) are not well described by DFT

methods. However, this is not sufficient to explain the deviation of calculated parameters from the experimental data. Some other factors, such as the DFT function, the size of the plane wave basis set, or the quality of the PAW atomic pseudopotentials, have effects on the accuracy of the calculations. The small shrinking of the cell volume in our calculations is the result of the optimization procedure used. We performed both cell shape and volume relaxation together with atomic position relaxation in one procedure. Such relaxation is conducted in the direction to minimize the so-called Pulay stress, which arises from the fact that the plane wave basis set is not complete with respect to the changes of volume that tend to decrease the cell volume during the relaxation. Thus, it is recommended that a large plane wave basis set (*i.e.* to define a large energy cutoff) is used for such relaxation. The energy cutoff of 400 eV used in our calculations is high enough, but still a very small cell volume decrease was observed. Another way to minimize Pulay stress-related problems is to perform calculations at different volumes using the same energy cutoff for each calculation, and to fit the final energies to an equation of state. In this way an equilibrium state with the minimal energy and corre-

Table 2a. Calculated relative energies for the structures described in Figure 2 with a unit-cell having fixed dimensions. Isomorphous substitutions of Fe(III), Mg(II) or Fe(II) for one Al in the unit-cell are considered as well as the structures with no substitutions.

Substitution	Excess charge ($|e|$)	Vacancy *trans*-OH		Vacancy *cis*-OH		ΔE^{d}
		Model[a]	$E_i - E_{min}$[b]	Model[a,c]	$E_i - E_{min}$[b]	
None[e]	0	−	−	−	−	4.9
Fe[III]/Al[III]	0	A1−4	0.0	A1,3	0.0	5.7
				A2,4	3.7	
Mg[II]/Al[III]	−1	A1−4	0.0	A1,3	0.0	−0.2
				A2,4	2.7	
		B2,3[f]	0.0	B1[f]	0.0	
				B2[f]	0.0	0.1
				B3[f]	12.6	
		B1,4[f]	8.0	B4[f]	13.5	
		C1−4	0.0	C1,3	0.0	0.1
				C2,4	5.5	
Fe[II]/Al[III]	−1	A1−4	0.0	A1,3	0.0	−0.4
				A2,4	0.8	
		B2,3[f]	0.0	B1[f]	4.2	
				B2[f]	0.0	−3.3
				B3[f]	17.3	
		B1,4[f]	10.6	B4[f]	14.8	
		C1−4	0.0	C1,3	0.0	3.2
				C2,4	4.2	

[a] Letters A−C and numbers 1−4 are illustrated in Figure 2.
[b] Relative energies (in kJ/mol) as differences between total electronic energies within the given group of four substitutions for each A−C model.
[c] *cis*-OH configuration of the substitution in positions 1 and 3, and *trans*-OH in positions 2 and 4.
[d] $\Delta E = E_{min}(cis) - E_{min}(trans)$ in kJ/mol.
[e] Pyrophyllite-like structure.
[f] Different distances of the Na^{+} cation to the substitutions in the positions 1−4 − see Figures 1 and 2.

sponding cell can be found. This type of calculation on pyrophyllite was also performed in this work for the case of 32 **k**-points, and the results are also given in Table 1. One can see that the calculated lattice vectors are slightly longer than the experimental ones, with the largest deviations (~0.3 Å) being with the *c* lattice parameter. This is in accord with the expected trends for DFT calculations. However, we have to stress that in this type of calculation the change of the cell volume is ~4% with respect to the experimental value. Table 1 also contains calculated mean values of bond lengths, and the deviations from the experimental values are very small (within 0.01 Å interval). Our results are in good agreement with other DFT calculations (Teppen *et al.*, 2002; Bruno *et al.*, 2006), and are closer to the experimental values than those presented in two additional theoretical DFT works (Refson *et al.*, 2003; Churakov, 2006).

Location of the vacancy in an (Al$_3$,M)Si$_8$O$_{20}$(OH)$_4$ isolated layer

Calculations of the relative energies for the vacant site with *cis*- and *trans*-OH coordination in an idealized isolated dioctahedral structure with fixed unit-cell dimensions are presented in Table 2a. These include situations with no layer charge (M = Al or Fe(III)), or a net charge of −1 per unit-cell (M = Mg or Fe(II)). In the case of negatively charged layers, three arrangements (A, B, C in Table 2a) for the interlayer cation were considered and these are illustrated in Figure 2. In case A no compensating cation was considered, in case B a Na$^+$ ion was placed close to the layer surface, and in case C this cation was placed in the middle of the vacuum above the layer, and its z-coordinate was kept fixed during the optimization procedure. The results of similar calculations in which the unit-cell parameters were allowed to relax at a constant cell volume are presented in Table 2b. Although relaxation of the unit-cell parameters produces a net stabilization, the relative energies of the various structures remain comparable to those from the calculations with fixed unit-cell dimensions. The relaxation energies are in the range 20−30 kJ/mol except for the pyrophyllite-like structure, where it is ~8.5 kJ/mol. Optimized unit-cell parameters, *a* and *b*, are presented in Table 3 for both types of OH coordination. These are slightly longer than the initial values used in the calculations with the fixed cell parameters (a = 5.162 Å and b = 8.980 Å). The column

Table 2b. Calculated relative energies for the structures described in Figure 2 with a unit-cell having optimized dimensions. Isomorphous substitutions of Fe(III), Mg(II) or Fe(II) for one Al in the unit-cell are considered as well as the structures with no substitutions.

Substitution	Excess charge ($|e|$)	Vacancy *trans*-OH		Vacancy *cis*-OH		ΔE^d
		Model[a]	$E_i - E_{min}$[b]	Model[a,c]	$E_i - E_{min}$[b]	
None[e]	0	−	−	−	−	6.6
Fe^{III}/Al^{III}	0	A1−4	0.0	A1,3	0.0	5.9
				A2,4	3.2	
Mg^{II}/Al^{III}	−1	A1−4	0.0	A1,3	0.0	1.4
				A2,4	1.4	
		B2,3[f]	0.0	B1[f]	0.0	1.3
				B2[f]	0.0	
		B1,4[f]	10.0	B3[f]	16.1	
				B4[f]	17.0	
		C1−4	0.0	C1,3	0.0	−0.6
				C2,4	6.3	
Fe^{II}/Al^{III}	−1	A1−4	0.0	A1,3	0.3	0.4
				A2,4	0.0	
		B2,3[f]	0.0	B1[f]	4.5	−2.5
				B2[f]	0.0	
		B1,4[f]	12.8	B3[f]	21.0	
				B4[f]	18.4	
		C1−4	0.0	C1,3	0.0	2.7
				C2,4	4.8	

[a] Letters A−C and numbers 1−4 are illustrated in Figure 2.
[b] Relative energies (in kJ/mol) as differences between total electronic energies within the given A−C group of four substitutions.
[c] *cis*-OH configuration of the substitution in positions 1 and 3, and *trans*-OH in the positions 2 and 4.
[d] $\Delta E = E_{min}(cis) - E_{min}(trans)$ in kJ/mol.
[e] Pyrophyllite-like structure.
[f] Different distances of the Na$^+$ cation to the substitutions in the positions 1−4 − see Figures 1 and 2.
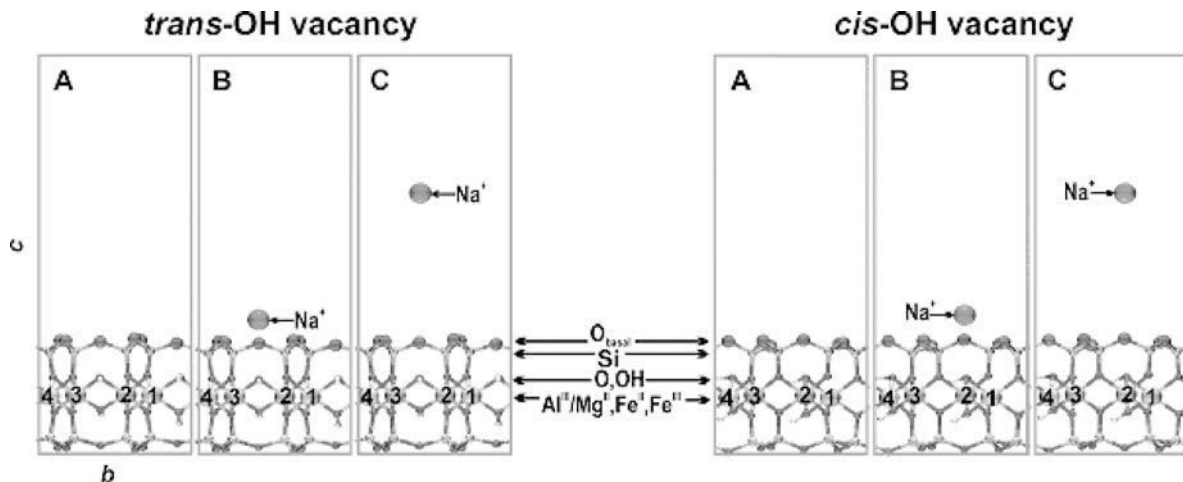
Figure 2. Arrangements considered for interlayer cations in structures with substitutions in the octahedral sheet $(Al_3M)Si_8O_{20}(OH)_4$. Letters A−C and numbers 1−4 correspond to models presented in Tables 2a and 2b.

in Tables 2a and 2b, labeled '$E_i - E_{min}$', shows the relative energies of the individual substitutions in each group of models A−C representing interlayer cation positions. The last column shows the differences in the total energies of the most stable structures with *trans*- and *cis*-OH coordination for the vacancy for each corresponding group of models A−C.

The magnitudes of the differences in energy for the two coordination arrangements for the vacancy are different for substitutions of tri- and divalent cation. For both divalent substitutions considered here, (Fe(II) and Mg(II)), the energy differences are very small ($\leqslant 3$ kJ/mol) for each interlayer cation situation (A, B, C); for Mg substitution the differences are almost negligible. This means that the stabilities of both types of structure are very similar. In contrast, with the substitution of Fe(III) for Al, the structure with the *trans*-OH coordination for the vacancy is more stable than that with a *cis*-OH vacancy coordination by

~6 kJ/mol (for the relaxed unit-cell, Table 2b). This is similar to the result with the pyrophyllite-like structure (*i.e.* no substitution), where the difference in the total energy between sites with *trans*- and *cis*-OH coordination for the vacancy is 6.6 kJ/mol, and is also in agreement with the experimental observation of *trans*-OH coordination for the vacancy in pyrophyllite (Lee and Guggenheim, 1981). With divalent ion substitutions and the interlayer Na$^+$ close to the surface, the structures in which the Na$^+$ is near to the substitution site are stabilized relative to those in which it is further away (see case B in Tables 2a, 2b). For example, model structures B1 and B4 for the vacancy with *trans*-OH, and Mg^{II}/Al^{III} substitution are less stable by 10 kJ/mol than models B2 and B3 (Table 2b). In B1 and B4 the distance between the Na$^+$ cation and the Mg^{2+} substitution is ~5.1 Å, whereas in models B2 and B3 this distance is ~4.1 Å. A similar situation occurs in the case of the *cis*-OH vacancy, but with the different arrangements of

Table 3. Optimized unit-cell parameters, *a* and *b*, for *cis*- and *trans*-OH vacancy coordination and for substitutions in both octahedral and tetrahedral sheets (values are taken for the position of the substitution with the lowest energy).

Substitution	Vacancy *trans*-OH			Vacancy *cis*-OH		
	Model	*a*	*b*	Model	*a*	*b*
None	−	5.249	9.045	−	5.226	9.086
Fe^{III}/Al^{III}	A1	5.290	9.105	A1	5.263	9.154
Mg^{II}/Al^{III}	A1	5.278	9.125	A1	5.258	9.164
	B2	5.266	9.114	B2	5.248	9.145
	C1	5.282	9.131	C1	5.257	9.185
Fe^{II}/Al^{III}	A1	5.294	9.140	A1	5.250	9.140
	B2	5.289	9.142	B2	5.292	9.139
	C1	5.262	9.120	C1	5.266	9.168
Al^{III}/Si^{IV}	A1	5.263	9.100	A1	5.247	9.120
	B2	5.255	9.054	B2	5.212	9.074
	C2	5.244	9.083	C2	5.235	9.092

the Na^+ cation relative to the substitution site. In models B1 and B2 the Na^+ cation is closer to the substitution than in models B3 and B4. Calculations using models with the Na^+ cation fixed in the middle of the vacuum (case C) gave identical results to those with model A. With the *trans*-OH coordination for the vacancy, all four possible substitution positions are energetically identical (due to symmetry), whereas with a *cis*-OH coordination, two types of substitution can be distinguished. The substituting cation can have either the *cis*-OH (positions 1,3) or *trans*-OH coordination (positions 2,4). Optimized structural parameters for all models with substitutions are longer than those of the pyrophyllite structure ('no substitution' in Table 3). It means that relative to the Al−O bonds, the substituting cations cause an expansion of the layer by elongating the bonds with oxygen atoms. This is because the ionic radius of Al^{3+} is smaller than the radii of each of the substituting cations. A similar observation was made by Sainz-Diaz *et al.* (2002). Differences in the cell parameters between different types of octahedral substitution are relatively small (~0.05 Å). The calculated cell parameters, *a*, are usually longer in the models with *trans*-OH vacancy coordination than in those where the vacancy has *cis*-OH coordination, whereas for the cell parameter *b* they are shorter.

Location of the vacancy in an $Al_4(Si_7T)O_{20}(OH)_4$ isolated layer

Note that the situation where T = Si is identical to that where M = Al in the previous section (*i.e.* a pyrophyllite-like layer) and its results are given in Tables 2a and 2b. When T = Al, there is a net charge of −1 per unit-cell, as was obtained with a single substitution of a divalent ion in the octahedral sheet in the previous section. The results of the calculations on all structures using fixed unit-cell dimensions, and structures where the unit-cell dimensions were allowed

to relax are presented in Tables 4a and 4b, respectively. The structures of Tables 4a and 4b are the same as those of Tables 2a and 2b. Three groups of models were constructed and their structures are displayed in Figure 3. In case A, no compensating cation was used, in case B, the Na^+ cation was placed close to the tetrahedral sheet with the substitution and in the case C this cation was placed close to the opposite tetrahedral sheet (without substitution). In each case all four possible positions for substitution in the tetrahedral sheet were mapped. When the vacancy has *trans*-OH coordination, the four substitution positions with no compensating cation (A1−4) are virtually equivalent and no differences in energies were found (Table 4a and 4b). In corresponding models A1−4 for the *cis*-OH vacancy, a small energy difference (2.2. kJ/mol in Table 4b) was found between models A1/A3 and A2/A4 due to the different positions of the OH groups relative to the substitution. As was the case with octahedral substitutions, it is possible to distinguish energetic differences for models with the Na^+ cation close to the substitution defects (models B1−4 in Tables 4a and 4b). These differences result from the different distances between the Na^+ cation and the substitution in positions 1−4. However, these different distances have an origin in the structural distortions of the ideal symmetry of the tetrahedral sheet in contrast to the octahedral substitutions. Models with *cis*-OH coordination for the vacancy (B1−4) have different energies (Tables 4a and 4b). They can be distinguished according to the position of the tetrahedral Al with respect to the hydroxyl groups and the above-mentioned structural distortions in the tetrahedral sheet. Similar, but smaller, differences were found for models C where the Na^+ cation is on the opposite side of the tetrahedral sheet (Figure 3).

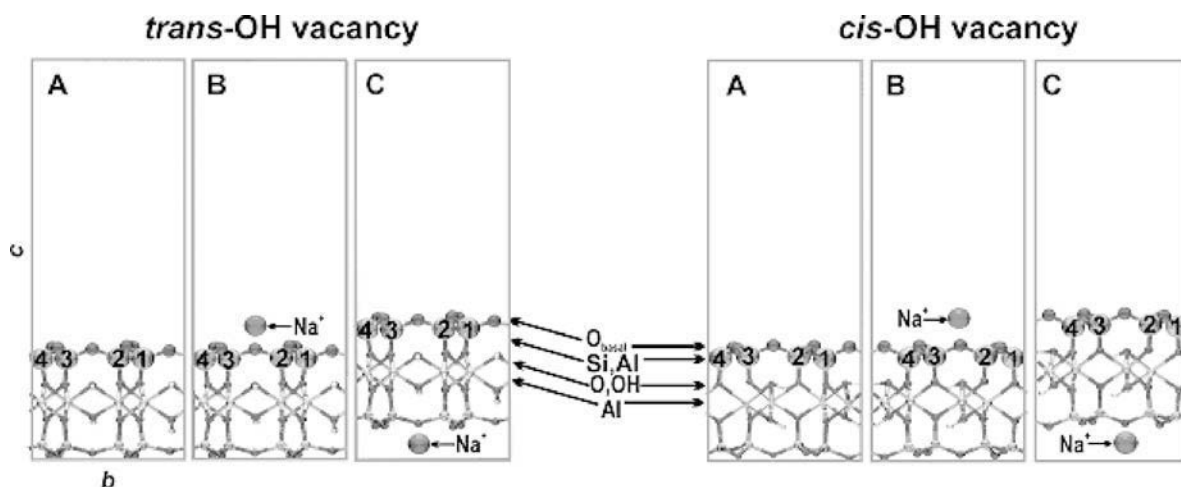The most significant finding in these calculations is that the arrangement with *cis*-OH coordination for the

Figure 3. Arrangements considered for interlayer cations in structures with substitutions in the tetrahedral sheet $Al_4(Si_7T)O_{20}(OH)_4$. Letters A−C and numbers 1−4 correspond to models presented in Tables 2a and 2b.

Table 4a. Calculated total relative energies for the structures described in Fig. 3 with a unit-cell having fixed dimensions. Isomorphous substitutions of Al for one Si in the unit-cell are considered in relation to the position of the interlayer cation.

Substitution	Excess charge ($|e|$)	Vacancy *trans*-OH		Vacancy *cis*-OH		ΔE^c
		Model[a]	$E_i - E_{min}$[b]	Model[a]	$E_i - E_{min}$[b]	
		A1−4	0.0	A1,3	0.0	−3.3
				A2,4	2.9	
		B1,4	6.9	B1	13.5	
				B2	0.0	−4.1
Al^{III}/Si^{IV}	−1	B2,3	0.0	B3	6.7	
				B4	19.8	
		C1,4	1.1	C1	0.7	
				C2	0.0	−8.4
		C2,3	0.0	C3	3.1	
				C4	5.8	

[a] Letters A−C and numbers 1−4 are illustrated in Figure 3.
[b] Relative energies (in kJ/mol) as differences between total electronic energies within the given A−C group of four substitutions.
[c] $\Delta E = E_{min}(cis) - E_{min}(trans)$ in kJ/mol.

Table 4b. Calculated total electronic energies and relative energies for the structures described in Figure 3 with a unit-cell having optimized dimensions. Isomorphous substitutions of Al for one Si in the unit-cell are considered in relation to the position of the interlayer cation.

Substitution	Excess charge ($|e|$)	Vacancy *trans*-OH		Vacancy *cis*-OH		ΔE^c
		Model[a]	$E_i - E_{min}$[b]	Model[a]	$E_i - E_{min}$[b]	
		A1−4	0.0	A1,3	0.0	−0.9
				A2,4	2.2	
		B1,4	4.8	B1	12.2	
				B2	0.0	−3.3
Al^{III}/Si^{IV}	−1	B2,3	0.0	B3	6.7	
				B4	17.1	
		C1,4	1.3	C1	0.7	
				C2	0.0	−8.4
		C2,3	0.0	C3	4.2	
				C4	6.7	

[a] Letters A−C and numbers 1−4 are illustrated in Figure 3.
[b] Relative energies (in kJ/mol) as differences between total electronic energies within the given A−C group of four substitutions.
[c] $\Delta E = E_{min}(cis) - E_{min}(trans)$ in kJ/mol.

vacancy is more stable than that with *trans*- coordination in each of the situations considered. Similar results were obtained for calculations with fixed or optimized unit-cell dimensions. In contrast to octahedral substitutions, changes in unit-cell parameters are minimal compared with those of the unsubstituted structure (Table 3). This is a paradox because the Al^{3+} cation has a larger ionic radius than Si^{4+} and causes a significant expansion of the AlO$_4$ tetrahedra. However, the structural stress is relaxed by deformation of the plane of basal oxygen atoms in the direction perpendicular to this plane.

DISCUSSION

These calculations do not provide a definitive answer to the question as to whether the vacancy in dioctahedral phyllosilicates has *cis*- or *trans*-OH coordination. Indeed, they indicate that the energy differences between the two situations are relatively small and dependent on the origin of the layer charge and the chemical nature of the cationic substituents in the structures. In the present work we found that for a structure in which the layer charge is derived solely from substitution of Al for Si in the tetrahedral sheet, the most stable situation is one in which the vacancy has *cis*-OH coordination although differences in energies are small. Similarly, a greater stability for configurations with *cis*-OH coordination for vacancies was found for Fe(III)-for-Al substitution in the octahedral sheet. In contrast, negligible differences were found for divalent substitutions (Mg(II), Fe(II)) in the octahedral sheet, indicating that both configurations are energetically equivalent.

We can conclude that in phyllosilicates where the layer charge is derived from Al for Si substitutions, structures with *cis*-OH vacancy coordination will prevail. However, this will not necessarily be the situation when other trivalent ions (*e.g.* Fe(III)) substitute in the tetrahedral sheet. Experimental evidence for nontronites, for example, indicates that vacancies are at sites with *trans*-OH coordination (Manceau *et al.*, 2000). This was also found in the present work for Fe(III) substitution in octahedral sites, but situations in which there is >1Fe/unit-cell were not considered here.

The present calculations indicate that in the absence of any isomorphous substitution, the $Al_4Si_8O_{20}(OH)_4$ structure with trans-OH coordination for the vacancy is favored by ~7 kJ/mol in agreement with the structure reported by Lee and Guggenheim (1981). Fe(III) substitution for Al in octahedral sites produces a similar stabilization of the structure, whereas in the situation with divalent ion substitution in the octahedral sheet, the energy of the structure with *cis*-OH coordination for the vacancy is similar to that with *trans*-OH coordination, and in some cases actually more stable. Thus, because many phyllosilicate minerals have structures in which the net charge is derived from a combination of octahedral and tetrahedral substitutions, it is unlikely that the vacant site will have the same coordination in all structures and domain (clustering) effects will probably occur. In this respect our conclusions are similar to those of Sainz-Diaz *et al.* (2001b) for calculations using transferable empirical interatomic potentials. Those authors found that the *cis*-OH vacancy configuration was most stable at the smectite end of the illite-smectite series and the *trans*-OH vacancy configuration was most stable in structures with high Mg^{2+} or Fe^{3+}. Our theoretical results are also consistent with the experimental data which shows Al-rich smectites having vacancies with *cis*-OH coordination (Drits, 2003).

We have found that the interlayer Na^+ cation, which compensates the negative charge on the aluminosilicate layer, is preferably localized close to the substitution site, irrespective of whether the substitution is in the tetraheral or octahedral sheet. In case of tetrahedral substitutions, different distances between the Na^+ cation and the substitution site result from structural distortions of the tetrahedral sheet. The energy stabilization of the Na^+ localization is between 7 and 20 kJ/mol. Thus it is expected that in dry phyllosilicates, the interlayer cations will move to the sites directly connected to the isomorphous substitutions. (It is interesting to compare this result with that for vermiculite, where the most stable structures are those having the Mg^{2+} cation closest to non-substituted tetrahedral site (Tunega and Lischka, 2003). However, in vermiculite the Mg^{2+} cations are hydrated and H bonds are the dominant interactions with the aluminosilicate layers).

Although configurations with the Na^+ cation close to the substitution site are the most stable for substitutions in both the octahedral and tetrahedral sheets, the distribution and localization of the net atomic charge is different for the two situations. This is shown in Table 5, where atomic charges of the basal oxygen atoms obtained by Mulliken population analyses are presented. This Table compares atomic charges for the model having no substitution with those for model A2 in Table 2b and model A4 in Table 4b. As expected, the basal oxygen atoms have more negative charges in models with substitutions than in the model with no substitution. However, the charge distributions are different for octahedral and tetrahedral substitutions. In the case of octahedral substitution, the excess negative charge is almost evenly delocalized over all basal surface atoms, whereas in the case of Al substitution in the tetrahedral sheet, the basal oxygen atoms directly bound to the Al substitution have the highest negative charges, although the differences in charges are small. The atomic labeling used in Table 5 and the localization of both the octahedral and tetrahedral substitutions are shown in Figure 4. There is no significant difference in the charge distribution between models with *trans*- and *cis*-OH coordination for the vacancy. Similar results were also obtained for Fe(II) substitution in the octahedral sheet, but these are not presented in Table 5.

Finally, one should consider the question as to why one should use *ab initio* methods for these calculations, when previous work using empirical interatomic potentials has provided good agreement with experiment. The

Table 5. Mulliken atomic charges calculated for the models shown in Figure 4.

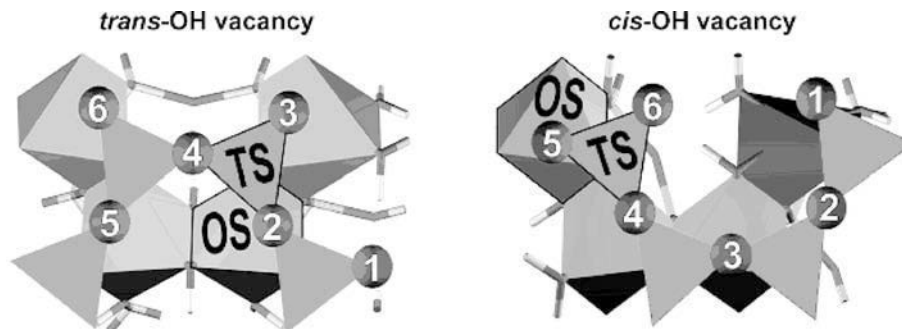| Model	O_{basal}					
	1	2	3	4	5	6
Vacancy *trans*-OH						
No substitution	−0.63	−0.64	−0.64	−0.63	−0.64	−0.64
A2: oct. Mg^{II}/Al^{III}	−0.65	−0.67	−0.67	−0.66	−0.66	−0.65
A4: tet. Al^{III}/Si^{IV}	−0.63	−0.66	−0.67	−0.65	−0.65	−0.64
Vacancy *cis*-OH						
No substitution	−0.65	−0.66	v0.65	−0.65	−0.65	−0.66
A2: oct. Mg^{II}/Al^{III}	−0.67	−0.67	−0.65	−0.66	−0.67	−0.68
A4: tet. Al^{III}/Si^{IV}	−0.65	−0.65	−0.67	−0.68	−0.66	−0.67

Figure 4. Nomenclature for the labeling of the basal oxygen atoms used in Table 5. Octahedral and tetrahedral substitution sites are also labeled.

principal reason is that empirical potentials are 'empirical'; they are non-rigorous, and there is always a question as to what extent results are transferable between samples. Also, when experimental data are used in the derivation of these potentials, they will always be subject to any errors associated with those data. For example, with clay minerals there are generally appreciable errors associated with determinations of chemical composition and layer charges, and these errors are compounded by the presence of impurities, even in reference specimens (Laird, 1994). However, it is such data that are used to generate empirical formulae for individual specimens. Generally, atoms assigned to the oxygen framework are then located in the following manner (see Čicel and Komadel, 1994, for example):

(1) All Si atoms are placed in sites with tetrahedral coordination.

(2) Al is placed in any tetrahedral sites not occupied by Si (if there is insufficient Al to fill all of these sites, then Fe(III) is also used).

(3) The remaining cations are placed in the sites with octahedral OH coordination.

This procedure assumes that there are no vacancies in tetrahedral cation sites. It can also be seen that the reliability of the information on the origin of the structural charge is completely dependent on the reliability of the analytical determinations, and is hence a source of major weakness in theoretical work aimed at simulating properties of experimental samples. Problems can arise as a result of:

(1) errors in the analytical determinations of the major elements

(2) the unrecognized presence of minor elements

(3) physical measurements being performed on different specimens to the analytical determinations

(4) the presence of minor, undetected, amounts of impurity phases.

Indeed, all of the above-mentioned problems are to be expected with clay minerals and it seems remarkable that theoretical work using empirical potentials should show good agreement with experiments. Extreme caution should be exercised in extrapolating results obtained with empirical models to samples with other composi-

tions because of the problems identified above. Nevertheless, the empirical approach can still be extremely valuable if combined with *ab initio* methods. The latter are able to determine short-range substitutional effects, whilst the former adds the potential for modeling and understanding large-scale phenomena.

Because the energy differences between structures are relatively small, on energy considerations alone it would seem likely that a range of structures could be present in any natural specimen (*i.e.* long-range disorder would be expected to be common). Kinetic rather than thermodynamic processes could, however, be the factors which determine which structure forms in nature. On the other hand, if thermodynamic processes dominate, then the Boltzmann equation predicts that the various structures might be expected to be present at levels that relate to their relative energies and formation temperatures.

In future work, it is our intention to apply *ab initio* calculations to the interpretation of physical data, which is essentially the reverse process of that used in the calculations using empirical parameters. We are especially interested in developing a comprehensive understanding of the Mössbauer spectra of aluminosilicate minerals, a problem that has been the source of considerable controversy for many years. Indeed, ~30 y ago, Goodman (1976) used a Monte Carlo method in an attempt to determine the lattice contribution to the electric field gradient (efg) distributions in dioctahedral micas. Here, as in later work, each atom was assigned full integral charges. Electronic contributions to the efg were not evaluated in that work and they were assumed to be identical for each site. Thus these calculations are only relevant to spectra recorded at very low temperatures. Nevertheless, they suggested that the distribution of the cations was non-random, as has subsequently been found experimentally.

CONCLUSIONS

In contrast to papers by Sainz-Diaz and co-workers, we separated the effects of substitutions in octahedral and tetrahedral positions on the layer structure of

smectites and its energetic stability. Only small energy differences are observed between the dioctahedral layer-silicate structures in which the vacancy has *cis-* or *trans-*OH coordination. Thus, many natural mineral specimens will probably contain a mixture of structures. This could be a major reason for the long-standing controversy as to which is the correct structural arrangement for this group of minerals. In our present calculations, we found that the structure with *trans-*OH coordination for the vacancy was the more stable only if the layer charge was derived from octahedral substitution with the trivalent Fe(III) cation. In other structures with divalent cations substituting for Al in octahedral sites, the arrangements with *trans-* and *cis-*OH coordination for the vacancy are energetically equivalent and their stabilities are virtually identical. Tetrahedral substitution of Al for Si invariably led to the arrangement with *cis-*OH coordination for the vacancy being the more stable. All of the structures with compensating cations are additionally stabilized when the interlayer cation is near to the site of substitution. The net layer charge is distributed over the basal oxygens differently for octahedral and tetrahedral substitutions. While in former structures the charge is near regularly delocalized over the basal oxygen atoms, in the latter structures the charge is localized on those oxygen atoms directly bound to the Al substitution.

ACKNOWLEDGMENTS

REFERENCES

Bailey, S.W. (1980) Structures of layer silicates. Pp. 1−123 in: *Crystal Structure of Clay Minerals and their X-ray Identification* (G.W. Brindley and G. Brown, editors). Monograph **5**, Mineralogical Society, London.

Benco, L., Tunega, D., Hafner, J. and Lischka, H. (2001) *Ab-initio* density-functional theory applied to the structure and proton dynamics of clays. *Chemical Physics Letters*, **333**, 479−484.

Blöchl, P.E. (1994). Projector augmented-wave method. *Physics Review B*, **50**, 17953−17979.

Bosenick, A., Dove, M.T., Myers, E.R., Palin, E.J., Sainz-Diaz, C.I., Guiton, B., Warren, M.C., Craig, M.S. and Redfern, S.A.T. (2001) Computational methods for the study of energies of cation distributions: applications to cation-ordering phase transitions and solid solutions. *Mineralogical Magazine*, **65**, 193−219.

Botella, V., Timon, V., Escamilla-Roa, E., Hernandez-Laguna, A. and Sainz-Diaz. C.I. (2004) Hydrogen bonding and vibrational properties of hydroxy groups in the crystal lattice of dioctahedral clay minerals by means of first principles calculations. *Physics and Chemistry of Minerals*, **31**, 475−486.

Bridgeman, C.H., Buckingham, A.D., Skipper, N.T. and Payne, M.C. (1996) *Ab-initio* total energy study of uncharged 2:1 clays and their interaction with water. *Molecular Physics*,

89, 879−888.

Bruno, M., Prencipe, M. and Valdre, G. (2006) *Ab initio* quantum-mechanical modeling of pyrophyllite [Al$_2$Si$_4$O$_{10}$(OH)$_2$] and talc [Mg$_3$Si$_4$O$_{10}$(OH)$_2$] surfaces. *Physics and Chemistry of Minerals*, **33**, 63−71.

Churakov, S.V. (2006) *Ab initio* study of sorption on pyrophyllite: structure and acidity of the edge sites. *Journal of Physical Chemistry B*, **110**, 4135−4146.

Čicel, B. and Komadel, P. (1994) Structural formulae of layer silicates. Pp. 114−136 in: *Quantitative Methods in Soil Mineralogy* (J.E. Amonette and L.W. Zelazny, editors). Soil Science Society of America, Inc., Madison, Wisconsin, USA.

Cuadros, J., Sainz-Diaz, C.I., Ramirez, R. and Hernández-Laguna, A. (1999) Analysis of Fe segregation in the octahedral sheet of bentonitic illite-smectite by means of FT-IR, ^{27}Al MAS NMR and reverse Monte Carlo simulations. *American Journal of Science*, **299**, 289−308.

Drits, V.A. (2003) Structural and chemical heterogeneity of layer silicates and clay minerals. *Clay Minerals*, **38**, 403−432.

Drits, V.A., Lindgreen, H., Salyn, A.L., Ylagan, R. and McCarty, D.K. (1998) Semiquantitative determination of *trans-*vacant and *cis-*vacant 2:1 layers in illites and illite-smectites by thermal analysis and X-ray diffraction. *American Mineralogist*, **83**, 1188−1198.

Goodman, B.A. (1976) The effect of lattice substitutions on the derivation of quantitative site populations from the Mössbauer spectra of 2:1 layer-lattice silicates. *Journal of Physics (Paris), Colloquium C6*, **37**, 819−823.

Hobbs, J.D., Cygan, R.T., Nagy, K.L., Schultz, P.A. and Sears, M.P. (1997) All atom *ab initio* energy minimization of the kaolinite crystal structure. *American Mineralogist*, **82**, 657−662.

Kresse, G. and Furthmüller, J. (1996) Efficiency of *ab-initio* total energy calculations for metals and semiconductors using a plane-wave basis set. *Journal of Computers in Mathematics and Science*, **6**, 15−50.

Kresse, G. and Hafner, J. (1993) *Ab initio* molecular dynamics for open-shell transition metals. *Journal of Physical Chemistry B*, **48**, 13115−13118.

Kresse, G. and Joubert, D. (1999) From ultrasoft pseudo-potentials to the projector augmented-wave method. *Physical Review B*, **59**, 1758−1775.

Laird, D.A. (1994) Evaluation of the structural formula and alkylammonium methods of determining layer charge. Pp. 80−103 in: *Layer Charge Characteristics of 2:1 Silicate Clay Minerals* (A.R. Mermut, editor). CMS Workshop Lectures, **6**, The Clay Minerals Society, Aurora, Colorado.

Lee, J.H. and Guggenheim, S. (1981) Single-crystal X-ray refinement of pyrophyllite-1Tc. *American Mineralogist*, **66**, 350−357.

Manceau, A., Lanson, B., Drits, V.A., Chateigner, D., Gates, W.P., Wu, J., Huo, D. and Stucki, J.W. (2000) Oxidation-reduction mechanism of iron in dioctahedral smectites: I. Crystal chemistry of oxidized reference nontronites. *American Mineralogist*, **85**, 133−152.

McCarty, D.K. and Reynolds, R.C. (1995) Rotationally-disordered illite/smectite in Paleozoic K-bentonites. *Clays and Clay Minerals*, **43**, 271−284.

McConnell, J.D.C., De Vita, A., Kenny, S.D. and Heine, V. (1997) Determination of the origin and magnitude of Al/Si ordering enthalpy in framework aluminosilicates from *ab initio* calculations. *Physics and Chemistry of Minerals*, **25**, 15−23.

Monkhorst, H.J. and Pack, J.D. (1976) Special points for Brillouin-zone integrations. *Physical Review B*, **13**, 5188−5192.

Morris, H.D., Blank, S. and Ellis, P.D. (1990) 27-Al NMR

spectroscopy of iron-bearing montmorillonite clays. *Journal of Physics and Chemistry*, **94**, 3121−3129.

Palin, E.J., Dove, M.T., Hernandez-Laguna, A. and Sainz-Diaz, C.I. (2004) A computational investigation of the Al/Fe/Mg order-disorder behavior in the dioctahedral sheet of phyllosilicates. *American Mineralogist*, **89**, 164−175.

Perdew, J.P. and Wang, Y. (1992) Accurate and simple analytic representation of the electron-gas correlation energy. *Physical Review B*, **45**, 13244−13249.

Perdew, J.P. and Zunger, A. (1981) Self-interaction correction to density-functional approximations for many-electron systems. *Physical Review B*, **23**, 5048−5079.

Refson, K., Park, S.-H. and Sposito, G. (2003) *Ab initio* computational crystallography of 2:1 clay minerals: 1. Pyrophyllite-1Tc. *Journal of Physical Chemistry B*, **107**, 13376−13383.

Sainz-Diaz, C.I., Cuadros, J. and Hernández-Laguna, A. (2001a) Analysis of cation distribution in the octahedral sheet of dioctahedral 2:1 phyllosilicates by using inverse Monte Carlo methods. *Physics and Chemistry of Minerals*, **28**, 445−454.

Sainz-Diaz, C.I., Hernández, A. and Dove, M.T. (2001b) Modelling of dioctahedral 2:1 phyllosilicates by means of transferable empirical methods. *Physics and Chemistry of Minerals*, **28**, 130−141.

Sainz-Diaz, C.I., Hernández, A. and Dove, M.T. (2001c) Theoretical modelling of *cis*-vacant and *trans*-vacant configurations in the octahedral sheet of illites and smectites. *Physics and Chemistry of Minerals*, **28**, 322−331.

Sainz-Diaz, C.I., Timon, V., Botella, V., Artacho, E. and Hernández-Laguna, A. (2002) Quantum mechanical calculations of dioctahedral 2:1 phyllosilicates: Effect of octahedral cation distributions in pyrophyllite, illite and smectite. *American Mineralogist*, **87**, 958−965.

Sainz-Diaz, C.I., Palin, E.J., Hernández-Laguna, A. and Dove, M.T. (2003a) Octahedral cation ordering of illite and smectite. Theoretical exchange potential determination and Monte Carlo simulations. *Physics and Chemistry of Minerals*, **30**, 382−392.

Sainz-Diaz, C.I., Palin, E.J., Dove, M.T. and Hernández-Laguna, A. (2003b) Monte Carlo simulations of ordering of Al, Fe, and Mg cations in the octahedral sheet of smectites and illites. *American Mineralogist*, **88**, 1033−1045.

Sainz-Diaz, C.I., Palin, E.J., Hernández-Laguna, A. and Dove, M.T. (2004) Effect of the tetrahedral charge on the order-disorder of the cation distribution in the octahedral sheet of smectites and illites by computational methods. *Clays and Clay Minerals*, **52**, 357−374.

Skipper, N.T., Chang, F.R.C. and Sposito, G. (1995) Monte-Carlo simulation of interlayer molecular-structure in swelling clay-minerals .1. Methodology. *Clays and Clay Minerals*, **43**, 285−293.

Smrčok, L. and Benco, L. (1996) *Ab initio* periodic Hartree-Fock study of lizardite 1T. *American Mineralogist*, **81**, 1405−1412.

Soler, J.M., Artacho, E., Gale, J.D., García, A., Junquera, J., Ordejón, P. and Sánchez-Portal, D. (2002) The SIESTA method for *ab initio* order-N materials simulation. *Journal of Physics: Condensed Matter*, **14**, 2745−2779.

Stixrude, L. and Peacor, D.R. (2002) First principles study of illite-smectite and implications for clay mineral systems. *Nature*, **420**, 165−168.

Stucki, J.W. (1988) Structural iron in smectites. Pp. 625−675 in: *Iron in Soils and Clay Minerals* (J.W. Stucki, B.A. Goodman and U. Schwertmann, editors). D. Reidel Publishing Co., Dordrecht, The Netherlands.

Teppen, B.J., Rasmussen, K., Bertsch, P.M., Miller, D.M. and Schäfer, L. (1997) Molecular dynamics modeling of clay minerals. 1. Gibbsite, kaolinite, pyrophyllite, and beidellite. *Journal of Physical Chemistry B*, **445**, 1579−1587.

Teppen, B.J., Yu, C.-H., Newton, S.Q., Miller, D. and Schäfer, L. (2002) Quantum molecular dynamics simulation regarding the dechlorination of trichloroethene in the interlayer space of the 2:1 clay mineral nontronite. *Journal of Physical Chemistry A*, **106**, 5498−5503.

Timon, V., Sainz-Diaz, C.I., Botella, V. and Hernández-Laguna, A. (2003) Isomorphous cation substitution in dioctahedral phyllosilicates by means of *ab initio* quantum mechanical calculations on clusters. *American Mineralogist*, **88**, 1788−1795.

Tsipursky, I. and Drits, V.A. (1984) The distribution of octahedral cations in the 2:1 layers of dioctahedral smectites studied by oblique-texture electron diffraction. *Clay Minerals*, **19**, 177−193.

Tunega, D. and Lischka, H. (2003) Effect of Si/Al ordering on structural parameters and the energetic stabilization of vermiculites − a theoretical study. *Physics and Chemistry of Minerals*, **30**, 517−522.

Wang, L., Zhang, M., Redfern, S.A.T. and Zhang, Z.Y. (2002) Dehydroxylation and transformations of the 2:1 phyllosilicate pyrophyllite at elevated temperatures: An infrared spectroscopic study. *Clays and Clay Minerals*, **50**, 272−283.